Filigree Shell Slabs

Material and Fabrication-aware Shape Optimisation for CFRP Coreless-wound Slab Components

Jorge Christie[1*], Serban Bodea[2], James Solly[1], Achim Menges[2], Jan Knippers[1]

[1] Institute of Building Structures and Structural Design, University of Stuttgart
Keplerstrasse 11, 70174 Stuttgart

[*] Corresponding author e-mail: j.christie@itke.uni-stuttgart.de

[2] Institute for Computational Design and Construction, University of Stuttgart

Abstract

In recent years, the coreless filament winding (CFW) technique has gained attraction due to its capacity to effectively realize large-scale lightweight building components out of fibre-reinforced composites. However, the sequential nature of its filament-based production process imposes a series of design constraints that restrain the use of this technique in new typologies and applications. The current research introduces a novel shape optimisation-to-fabrication method that expands the scope of CFW towards the production of load-bearing components for slabs. A multi-stage workflow is proposed, integrating parametric design, shape optimisation, stress-driven material layup, and fabrication to ensure a high level of consistency between form and materialization. The research is presented in two phases. The first phase explores the use of shape optimisation to comprehend the underlying logic of shell forms capable of performing under the specific requirements of the slab scenario. The second phase integrates the inherent conditions of the material, formwork system, and robotic filament winding process into a seamless design-to-manufacturing workflow. The research resulted in a 10.2 kg prototype of a slab load-bearing structure that withstood a load of 559 kg while spanning 2.7 m, demonstrating the effectiveness of the approach.

Keywords: Optimisation, form finding, fabrication-aware, coreless filament winding, composites, carbon fibre.

1 Introduction

The coreless filament winding (hereafter 'CFW') is an integrative design-to-fabrication method for producing large-scale lightweight structural building components using carbon and glass fibre-reinforced polymer composites. Since 2011 this technique has been the subject of continuous developments by the Institute of Computational Design and Construction (ICD) and the Institute of Building Structures and Structural Design (ITKE) at the Stuttgart University. CFW is a variant of the well-researched industry standard for core-based composite filament winding. It consists of sequentially wrapping uncured FRP fibres around a minimal, often skeletal formwork following a given path until the target shell structure is achieved. Once cured and tempered these structures achieve their maximal strength (Waimer et al. 2013). The use of minimal formwork is acknowledged as an effective approach to reducing the waste and demoulding issues often associated with full-size solid cores (Felbrich et al. 2017). Additionally, its automated fabrication process enables the integration with computational design, simulation and optimisation tools, offering a high degree of control over the mechanical behaviour of each component up to the fibre level (Dörstelmann et al. 2014).

Despite these advantages, the sequential fibre-based production process of CFW imposes a series of geometrical constraints that limit the scope of designs that are simultaneously performative and suitable for fabrication. Although these limitations have been successfully addressed for the development of load-bearing structures for enclosures, cantilevering canopies, long-span domes and vertical structures (**fig. 1**), there is still a gap in design methodologies to permit the expansion of CFW to new structural typologies and applications.

Figure 1: Previous work on load-bearing structures realized in coreless filament winding. (**a**) ICD/ITKE Research Pavilion 2012, (**b**) ICD/ITKE Research Pavilion 2013-14, (**c**) ICD/ITKE Research Pavilion 2016-17, (**d**) Elytra Pavilion 2016, (**e**) BUGA Fibre Pavilion 2019 [itke.uni-stuttgart.de], (**f**) Marshall Prado, UTK Filament Tower 2019 [Hadley Fruits].

The present paper outlines a novel design-to-fabrication method that aims to extend the scope of CFW towards the realization of load-bearing structures for slab components. In regards to the constraints imposed by the fabrication process and the particular requirements of the slab scenario, a tailored shape optimisation method is implemented to ensure the production of performative, windable shell designs. The research is introduced by a thorough revision of the design constraints

that emerge from the fabrications approach and the application case, and is followed by the description of the two phases of development of the shape optimisation approach. The first phase implements a fabrication-agnostic shape optimisation aiming to identify the principles behind shell forms capable of performing under the given constraints. The outcome of this phase is a set of design principles that inform the development of "windable" slabs. The second phase implements a material-and-fabrication-aware shape optimisation, integrates it with a fibre optimisation module and generates the fabrication data for the realization and testing of a full-scale prototype. The actual implementation of the robotic fabrication of the component is out of the scope of the present research. In the context of this paper the term "roving" is used for naming a single bundle of fibre reinforcement filaments. When this roving is impregnated in resin, but still uncured and flexible, is referred to as (FRP or composite) "fibre", and once cured is called "strut".

2 Background

2.1 A tension-driven process

Unlike other additive manufacturing technologies, CFW is driven by mechanical pretension. Single or multiple continuous rovings are unrolled, passed through the resin bath, wound around anchor points, and consolidated in a process that constantly pulls the FRP fibre (**fig. 2a**). This tension is also what shapes CFW structures at various levels.

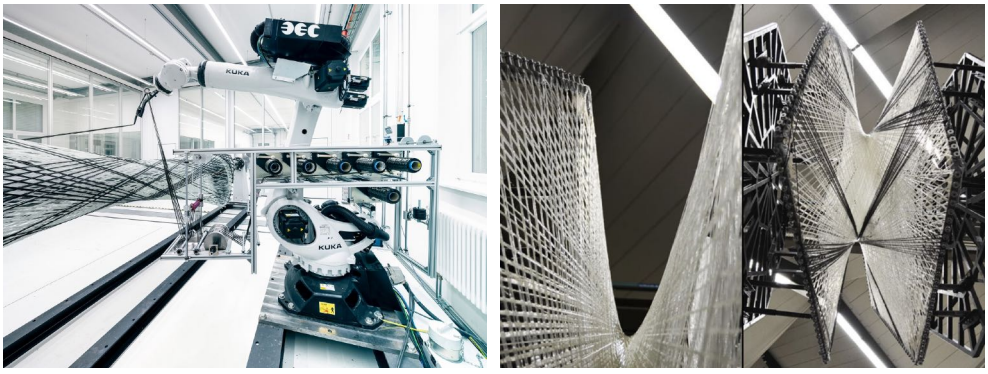

Figure 2: (**a**) Robotic filament winding setup for the BUGA Fibre project, (**b**) Hyperboloid-like component of ICD/ITKE 2013-14 showing a detail of the resulting lattice shell [itke.uni-stuttgart.de].

At fibre level, tension forces every FRP fibre spanning between anchor points or contact points with other fibres to be a straight, slender element. This slenderness accentuates as the structure becomes more material-efficient since the elements must span longer distances. Additionally, the pulling and handling of the UD

fibres result in variations on their cross-sections (Koslowski et al. 2017) that are further flattened in contact with crossing fibres and anchoring elements. This combination of slenderness and irregular cross-section makes the cured struts prone to buckle under axial compression before reaching their maximum compressive strength. Conversely, when subject to axial tension, the straightness of the struts allows them to profit from the full tensile capability of the material. Therefore, when aiming to maximize the material efficiency on CFW structures the designs should be steered towards a higher use of fibres in tension. At surface level, the formation of the shell-like lattice relies on the so-called fibre winding syntax, a systematic sequence of fibre placement (Prado et al. 2014). This sequence must ensure the crossing and pressing of the subsequent fibres to achieve the necessary fibre-to-fibre bonding for the composite action (Dörstelmann et al. 2014). As a result, the forming of a surface is a stepped process where, typically, the first set of fibres describes a ruled surface that is progressively shaped into an anticlastic surface (Waimer et al. 2013). Therefore, with CFW, complex geometries can only be accomplished as a combination of anticlastic surfaces (**fig. 2b**).

2.2 The formwork approach

In CFW, the formwork strategy strongly influences the final shape of the components. As seen in previous CFW-based works, structural shells have been produced using three main approaches: (1) in-crease curved formwork (**fig. 1a**), (2) in-edge linear formwork (**fig. 1b, d-f**), and (3) stay-in-place bending active plate formwork (**fig. 1c**). For the present research, the latter approach is selected. It consists of thin GFRP sheets that are elastically bent in position, fixed, and further reinforced by winding FRP fibres around it (Solly et al. 2018). Once cured, the shaped piece serves as the formwork for the subsequent surfaces. This approach presents several advantages: (1) it allows for fast and easy definition of curved formwork; (2) by custom shaping the plates through CNC processing, anchoring elements, placing marks and fixations can be integrated; and (3) by winding fibres around the curved plate hollow sections are created, improving the bending inertia and buckling strength of the component (**fig. 3a**).

2.3 Robotic Filament Winding

The configuration of the robotic winding set-up exerts great influence in the achievable form and dimensions of CFW structures, as observed by Felbrich et al. (2017). Typically, restrictions emerge from the reach of the robotic system and tooling, the potential collisions between them and the built structure, and from the approach to fibre feeding. The present research is based on installed capacities at the University of Stuttgart labs, including a Kuka KR 420 R3080 robotic arm mounted

on a KUKA Linear Axis of 10m long. A prepreg fibre feeding system mounted in the robotic end effector has been considered, allowing high degrees of freedom to the movements of the robotic arm. Given that the chosen formwork approach requires a fixed structure to shape the bending plates, the robot movements are restricted to one side of the structure (**fig. 3b**). Additionally, it was identified that, for the chosen CFW approach, free-form shapes can only be attained between two formwork edges. When intermediate creases are added, some shapes cannot be wound due to collisions with previously laid fibres.

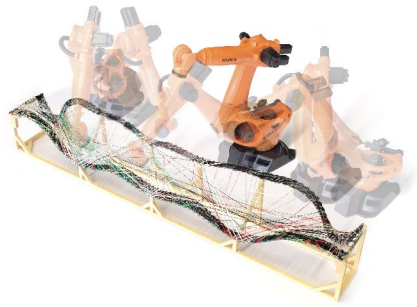

Figure 3: (**a**) Bending active stay-in-place FRP formwork for ITECH Pavilion 2016-17. Hollow sections in red [icd.uni-stuttgart.de], (**b**) Il. of the proposal for robotic fabrication of a slab component [il. by the authors].

2.4 Shells for slabs

When compared to shells used for enclosures, shells for slabs deal with a far more constrained scenario (**fig. 4**). Arguably, slabs must provide a horizontal plane on its walkable side. But flat planes don't easily interface with the curved surface of shells, requiring ribs or fillers to mediate between both geometries (**fig. 5a-b**). At the same time, space efficiency pushes shell designs to be as shallow as possible (high span, low rise) to fit more stories per building. But shallow shells exert an inversely proportional horizontal thrust to their supports (Engel 2007), inducing undesirable load to the walls and preventing the component to be self-supporting. This issue is commonly compensated by the addition of horizontal beams, tension ties or thick support walls, leading to less material-efficient and/or less elegant solutions. For this research, the horizontal thrust is aimed to be solved by making use of the shell's own form and fibre arrangement, so only vertical forces are transferred to the supports, as is the case for a typical prefabricated slab component.

Buckling has been acknowledged as one of the most critical failure modes for thin shell structures (e.g. Malek 2012; Williams 2014; Brandt-Olsen 2015) and FRP lattice shells are not the exception (Koslowski et al. 2017). Buckling on slab shells is traditionally addressed by adding stabilized filler as dead load (**fig. 5a**) and/or

incorporating stiffening ribs (**fig. 5b**). Yet another effective approach is the addition of local curvature (Malek 2012; Brandt-Olsen 2015; Malek and Williams 2017) (**fig. 5c**). This method has proven to improve buckling strength up to 8 times at minor volume increase expense (Malek 2012). Given the logic of form generation of CFW, this approach is deemed more suitable to the present research.

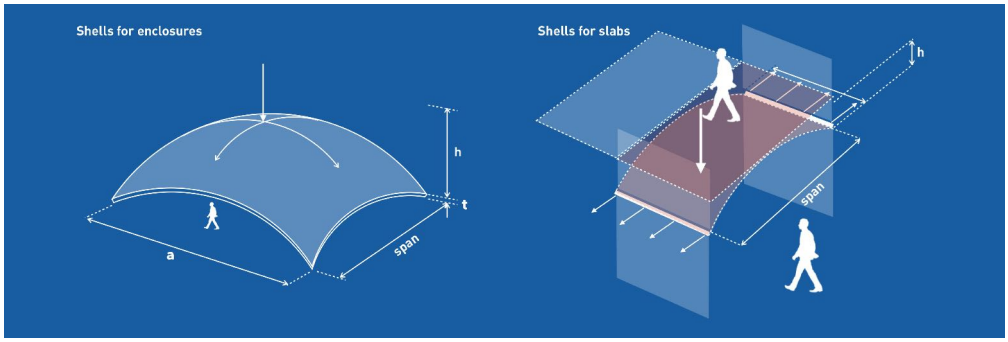

Figure 4: Comparative illustration of the design constraints of shells for enclosures and shells for slabs [il. by the authors].

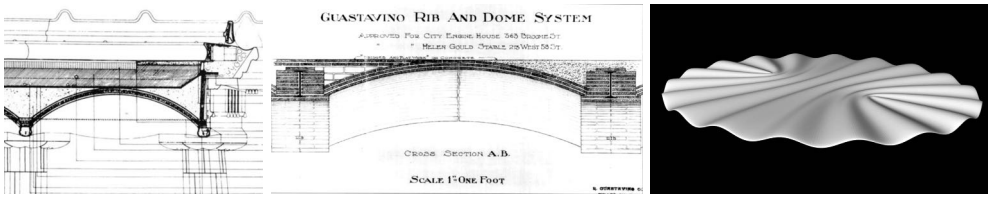

Figure 5: Strategies for dealing with buckling on shells for slabs: (**a**) Gaudí, Park Güell hypostyle room slab 1914 (fragment) [Rovira i Pey 1990], (**b**) Guastavino, Rib and Dome System 1902 [Collins Collection, Columbia University], (**c**) Corrugated plate [Malek and Williams 2017].

A review of the above mentioned design constraints that converge in the design of CFW slabs provides a good overview of the challenges of the implementation of the shape optimisation method. These constraints can be summarized as:

- CFW can only produce anticlastic surfaces (that typically derive from ruled surfaces).
- Material-efficient designs should promote the use of fibres in tension.
- The simulation of the formwork approach must describe the interaction between the bent plate and the wrapping fibres.
- A two-edged formwork ensures accessibility to the anchoring points for any given shell design.
- The shell must be form-found within a constrained span-to-rise design space.

- Horizontal thrust on the supports should be minimised.

- Buckling should be prevented, ideally by the use of local curvature and by keeping the spanning fibres within the range of the buckling length.

3 Methods

The research is based on a computational workflow implemented in the Rhino 6 / Grasshopper platform (McNeel 2018). It integrates custom Python algorithms developed by the authors, FE analysis performed in Karamba 3D 1.3.1 (Preisinger 2018), physics simulations carried out in Kangaroo 2.42 (Piker 2017), and the multi-objective optimisation algorithm Octopus 0.3.6 (Vierlinger 2015).

3.1 Phase 1: fabrication-agnostic shape optimisation

Shape optimisation is a suitable approach to find efficient shell forms when diverse -even conflicting- objectives must be concealed (Adriaenssens et al. 2014). During this phase, a structural shape optimisation workflow is implemented combining three modules: a CAGD-based surface generation (as described by Bletzinger and Ramm (2014), a finite element analysis (FEA), and a multi-objective genetic algorithm (MOGA). The surface generation is carried out by fitting a NURBS surface through an array of points of 5 x 1.2 m, whose Z position (except supports) is controlled by the MOGA between -20 cm and +40 cm from the support level. The support points are allowed to move in the span direction between -15 cm and +15 cm. The surface is then subjected to FEA as a continuous shell of 5 mm thickness and subjected to a distributed load of 4 kN/m^2 and gravity load. For this initial analysis, the CFRP material is considered isotropic. Two support conditions are tested: one capable of withstanding horizontal thrust (both hinged) and one that can't (one support pinned and the other a roller). From the analysis, the bending energy and tensile/compressive forces are obtained and fed to the MOGA. For comparison purposes, mass, support reactions, and deflection are also obtained. The optimisation objectives in the MOGA are set to minimise bending and prioritize solutions with higher tensile/compressive stresses ratio. The Pareto front solution space emerged from the optimisation loop offers a wide scope of shell designs to evaluate, facilitating the identification of form-performance patterns.

A series of seven different optimisation scenarios is evaluated, combining support conditions and maximum allowable height variation in relation to the supports (+40 / -20 cm, +20 / -40 cm). For comparison purposes, a compression-only design (+40 cm, support condition 1) and a 5 x 5 m sample (+40 / -20 cm, support condition 2) were evaluated. From comparative data and visual analysis was observed that:

▪ the support condition (pinned + roller), as expected, effectively steers the solutions towards near-zero horizontal thrust in the supports;

▪ local undulations on the surface of the samples provide significantly higher buckling strength compared to the compression-only design;

▪ the stresses flow mostly concentrated in the creases of the shell, comparable to corrugation behaviour. Towards the spanning edges this pattern becomes less clear (**fig. 6**);

▪ the performative samples can be described by a set of undulating counterbalancing creases in the spanning direction. An influence of a compressive catenary can be appreciated (**fig. 7a**).

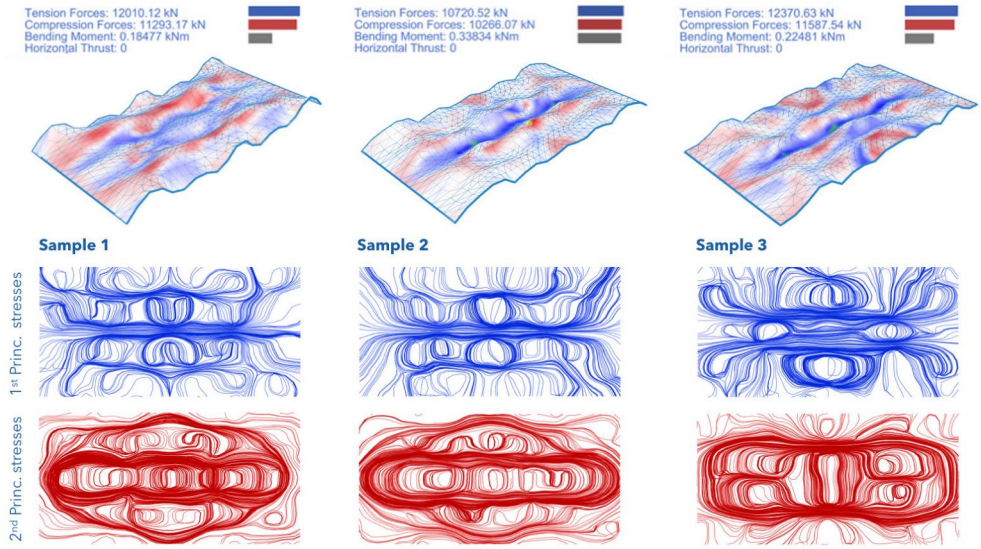

Figure 6: Comparison of three samples generated during the phase 1 of the development. Here the support points' displacement is deactivated [il. by the authors].

3.2 Phase 2: Embedding material and fabrication awareness

From simple visual analysis, it becomes evident that the complex shapes and abundant synclastic areas of the shells generated during Phase 1 are not suitable for CFW. Therefore, a "translation" strategy is required to transfer part of the mechanical effectiveness of these designs to windable forms. As previously observed, a persistent pattern of alternated undulating creases -where most stresses concentrated- was identified. Following this logic, the slab surface is discretised in a series of strips defined by couples of undulating curves (creases) connected by a "relaxed" ruled surface (infill) (**fig. 8**). Except for some singly curved areas on the creases, the whole component is described by anticlastic surfaces.

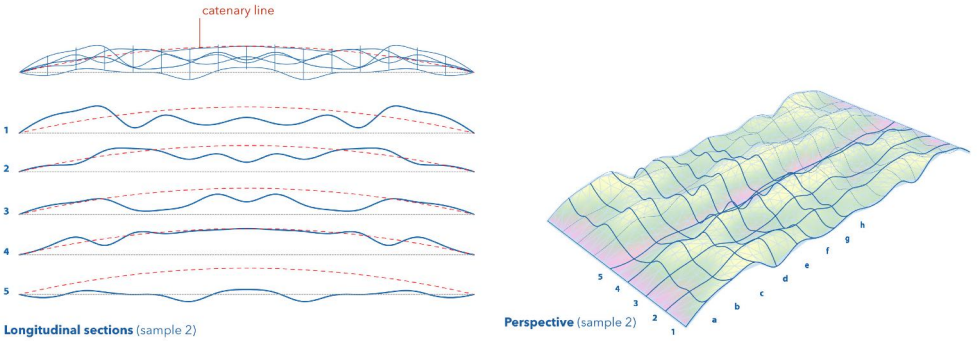

Figure 7: (**a**) Longitudinal sections of a sample. The influence of the catenary curve can be appreciated, (**b**) Perspective of the sample showing a depth color map and sections [il.s by the authors].

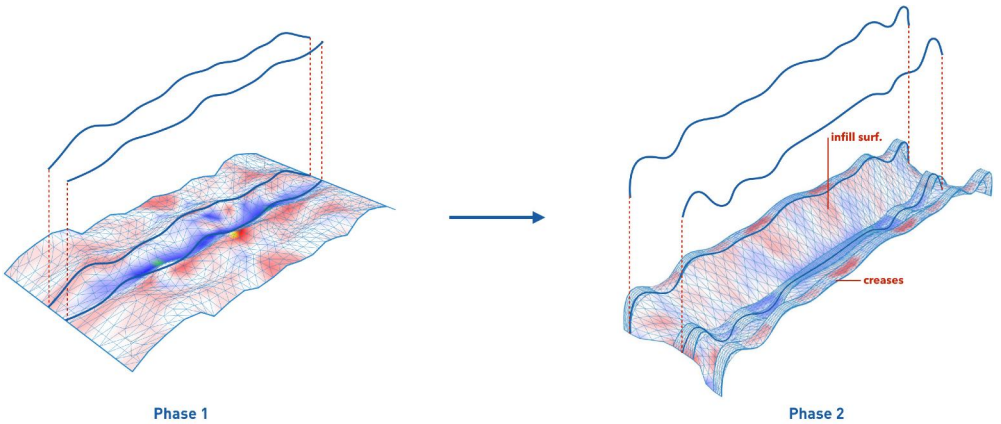

Figure 8: Translation strategy for the shell model generation from phase 1 (left) to phase 2 (right) [il. by the authors].

During phase 2 an integrated shape optimisation-to-fabrication workflow is proposed, articulating reflections concerning design, optimisation and fabrication within a common computational platform. It comprises three main modules seamlessly integrated: shape optimisation, fibre syntax generation/optimisation, and fabrication data (**fig. 9**).

3.3 Shape optimisation

Based on the translation strategy, a new shape optimisation loop is implemented, integrating a new shell model, FEA and a MOGA (**fig. 10**).

The shell model

Surface models have often been employed during the design phase of CFW lattice composite structures as a means for evaluating the global design and components' behaviour (Knippers et al. 2016; Koslowski et al. 2017; Solly et al. 2018). They

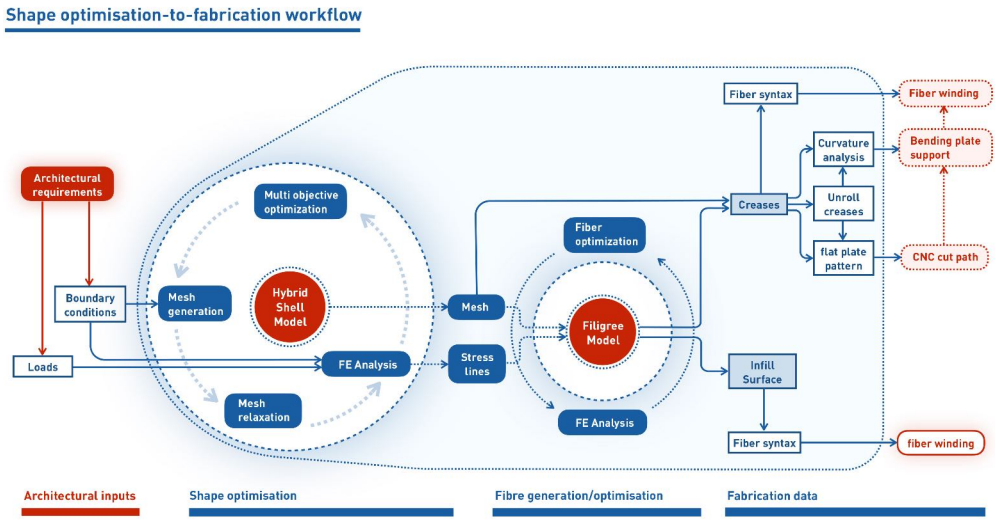

Figure 9: Shape optimisation-to-fabrication workflow. As architectural inputs the slab dimensions and loads required by the use are defined. The Shape optimisation module generates the hybrid shell model as described in 3.3.1, resulting in a mesh model and its principal stress lines. In the Fibre generation/optimisation module the fibre model is generated and iteratively optimised, retrieving the creases' mesh, the position of the infill fibres and data of their topographical relation. In the Fabrication data module the anchoring elements are added to the creases, whose curvature is analysed to place the supports for fabrication. The winding syntax is generated, as well as the CNC cutting path for the glass fibre and fabrication data for the support structure. The infill fibre syntax is generated using a pseudo-code based in topographical rules not described in the present work [il. by the authors].

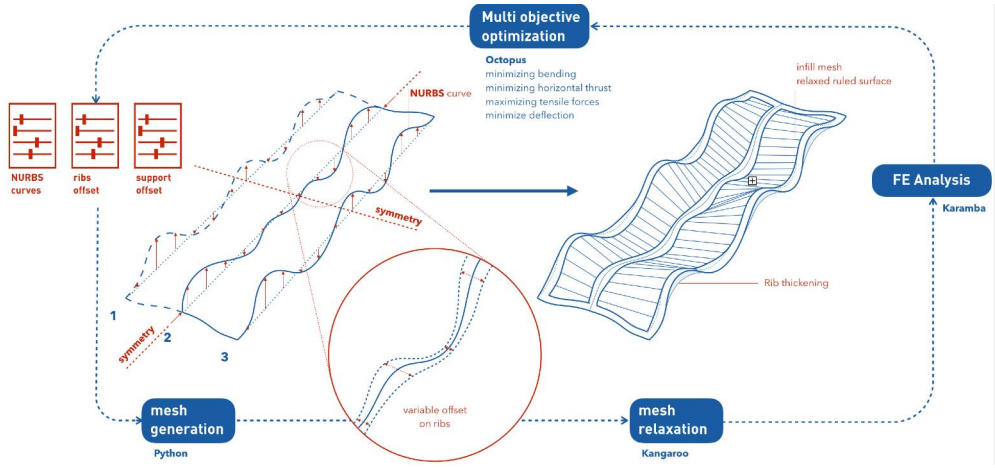

Figure 10: Fabrication-aware shape optimisation loop implemented [il. by the authors].

offer a more computationally efficient representation of the lattice surfaces than detailed fibre-level simulation models, yet still provide useful analysis results. These surfaces can be approximated by membrane-relaxation simulations (Solly et al. 2018) and further calibrated by comparison with physical models. Regardless of the efficiency of surface models, the integration of the fabrication-driven features

results in a significantly more complex model (hence computationally expensive) than the one used in phase 1. Therefore, the goal of the surface model is to provide reliable simulations while keeping its generation and analysis fast enough for an efficient optimisation iteration. A new shell component of 2.70 m of span and 0.80 m width is defined symmetric in both directions, (analogous to phase 1) resulting from the following sequence (illustrated in **fig. 10**):

a) generation of the control points for half the curve of each crease. The Z position of these points is controlled by the MOGA (-0.27 m to +27 m), defining the structural depth of the component and its relation with the supports;

b) generation of the support points. They are allowed to move in the span direction (-0.1 m to +0-1 m) controlled by the MOGA;

c) mirroring crease points and fitting a NURBS curve through them to define each crease;

d) definition of the plate's width by a variable offset from the initial curves controlled by the MOGA;

e) implementation of a custom meshing algorithm that generates a triangulated mesh with independent control for each edge direction;

f) generation of the crease mesh and relaxation;

g) generation of the infill mesh and relaxation.

From the steps mentioned above, the generation of the mesh for simulating the creases, the infill and their interaction are worth further explaining. The creases' shape results from the interaction of two elements with different forming behaviour: a GFRP plate that bends with single curvature and the wrapping fibres that adhere to the exterior side of the curved plate, while defining an anticlastic surface towards the interior (**fig. 11b**). Such interaction is estimated too computationally expensive for a collision-based simulation, therefore a geometric approximation is implemented. It comprises two relaxed copies of the crease mesh that are intersected and trimmed by the singly curved FRP plate and then merged (**fig. 11a**). Although the resulting mesh does not render the exact interaction of the two elements, its approximation is considered sufficient for the iterative shape optimisation (**fig. 11b**).

The free undulation of the creases that define the overall shape of the shell results in an infinite number of possible infill surface solutions. Likewise, given that the infill fibres are anchored to the exterior edges of the creases, the interaction between

both elements differs for each design. Possible infill-crease interaction cases are summarized in **fig. 12b**. An algorithm is developed to evaluate which interaction case applies to each anchoring point and assign a new point if required (**fig. 12b**).

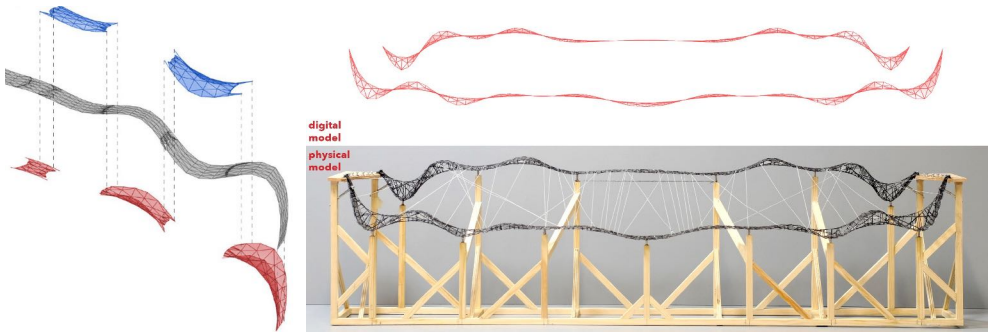

Figure 11: Crease mesh generation: (**a**) Detail of the surfaces intersected to create the mesh. In grey the GFRP plate, in blue and red, the wrapping fibres, (**b**) Comparison of the resulting mesh on top and a physical prototype on the bottom. [il. by the authors].

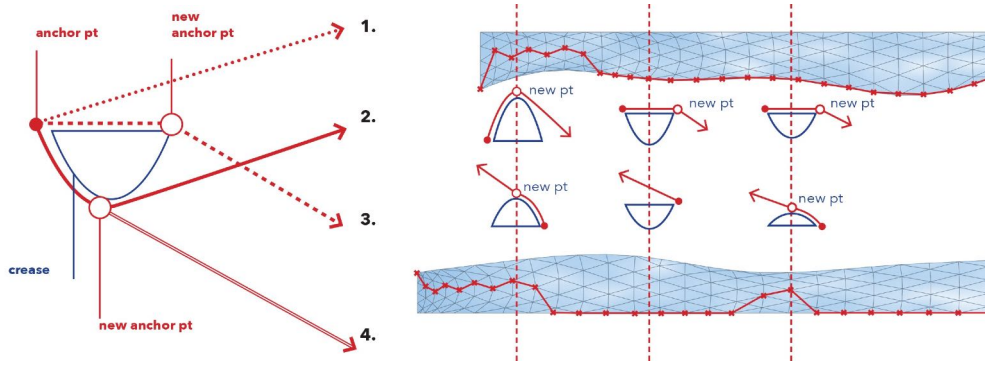

Figure 12: (**a**) The four possible crease-infill interaction cases. Cases 2 and 3 require assigning a new anchor point for the mesh creation, (**b**) Plan and sections showing how the algorithm reassigns anchor points based on the case evaluation [il. by the authors].

Once the new contact points are defined, the infill mesh is created. The custom meshing algorithm allows defining an appropriate resolution and selecting the diagonal edges of the mesh for relaxation, rendering an accurate representation of the surface.

Shell FEA and MOGA

The resulting shell model is analysed by FEA, retrieving both the necessary data for optimisation and the stress lines required to generate the fibre model. The setup of the FEA follows the same approach as phase 1 in terms of material, thickness, and support conditions (pinned + roller). A distributed load of 2.5 kN/m^2 and gravity load are applied (**fig. 13**). A shell analysis is performed retrieving bending energy, deflection, buckling and tension/compression ratio.

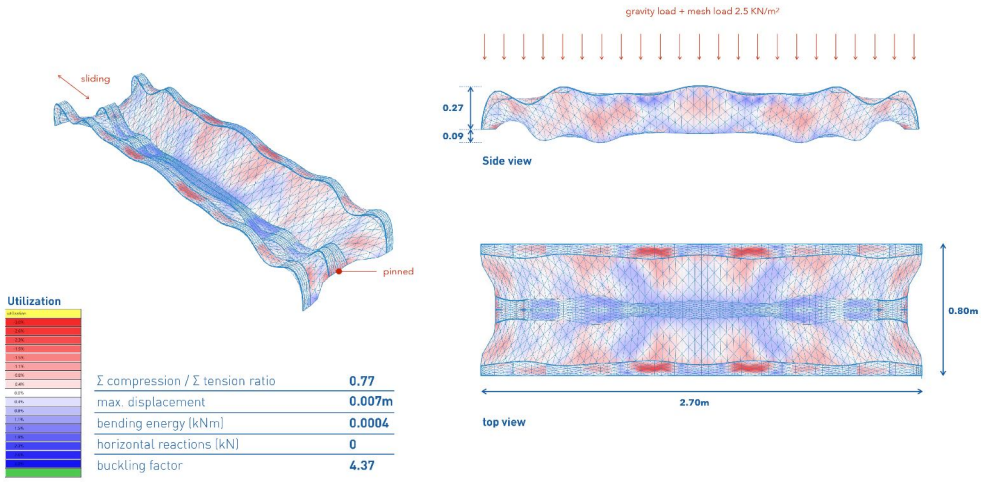

Figure 13: Hybrid shell model generated during the shape optimisation loop [il. by the authors].

With a similar aim than phase 1 the MOGA optimisation goals are set to maximize tension-compression ratio and minimise bending and deflection. As the support condition forces the generation of horizontal thrust-free solutions, this goal isn't included in the optimisation.

3.4 Fibre optimisation module

For the generation of the filigree model, a different strategy is used for the creases and the infill. The creases are directly translated from the mesh model to beam elements, generating a regular winding syntax that directly mimics the mesh of the element. For the infill surface, the curved trajectories of the principal stresses in the shell are translated into "windable" trajectories. This is accomplished by projecting each stress curve into a 2D plane, for later discretising and extending them to the boundaries of the projected surface. The obtained lines are then matched with the possible windable trajectories and projected back to the 3D surface (**fig. 14**). This simple process renders a pattern of windable curves where the stresses can effectively follow the original trajectories transferred from fibre to fibre (**fig. 15**). The fibre pattern is thus rebuilt as a network of beam elements spanning from each fibre intersection and fed into a new FEA module. Finally, the filigree structure is further optimized by culling under-stressed elements and performing a cross-section optimisation to define the amount of fibres per trajectory.

3.5 Fabrication data module

The fabrication data module generates the necessary information for the fabrication of the rigid formwork that fixes the GFRP plates in position, the cutting patterns of such plates (**fig. 16a**), and the winding instructions for both the creases and

the infill (**fig. 16a-b**). The prototype was fabricated by hand-winding the fibres following the sequence provided by the software. While this doesn't cast light over collision and singularity issues usually involved in complex robotic path planning nor over pretension control, hand wound prototypes are acknowledged to provide a good approximation to the resulting structure (Prado et al. 2014). The next phase of the project would be to transfer the fabrication information into robotic winding code.

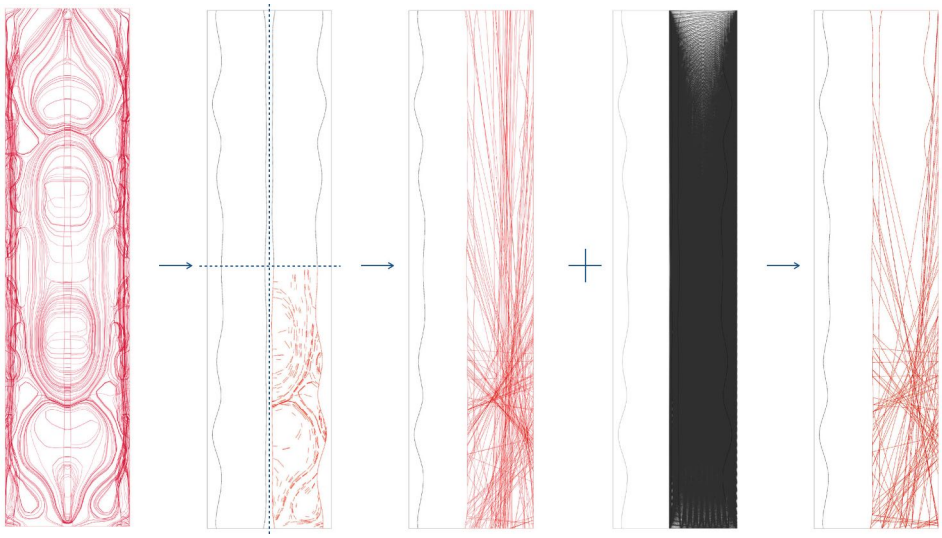

Figure 14: Example of the sequence for transferring from stress lines to stress-informed windable lines [il. by the authors].

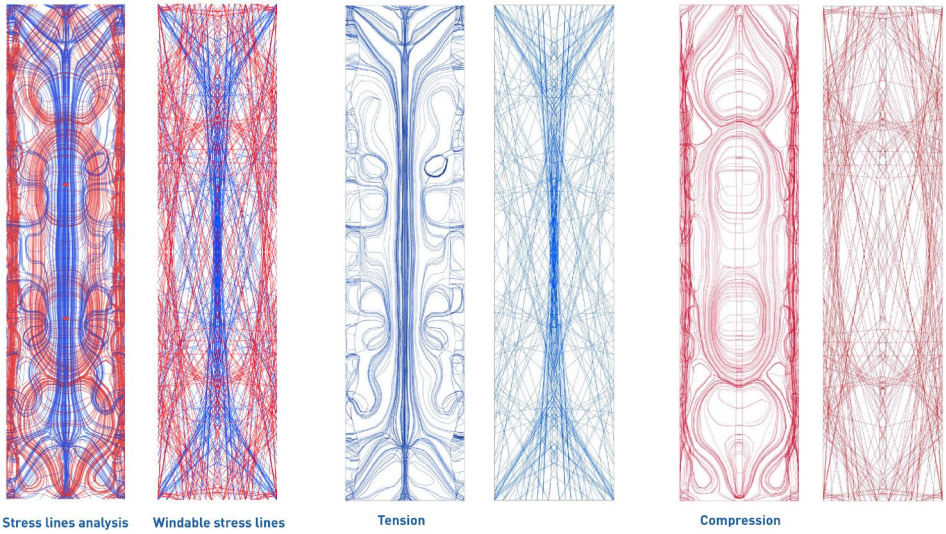

Figure 15: Comparison of stress lines (left) and stress-informed windable lines (right). From an intermediate design [il. by the authors].

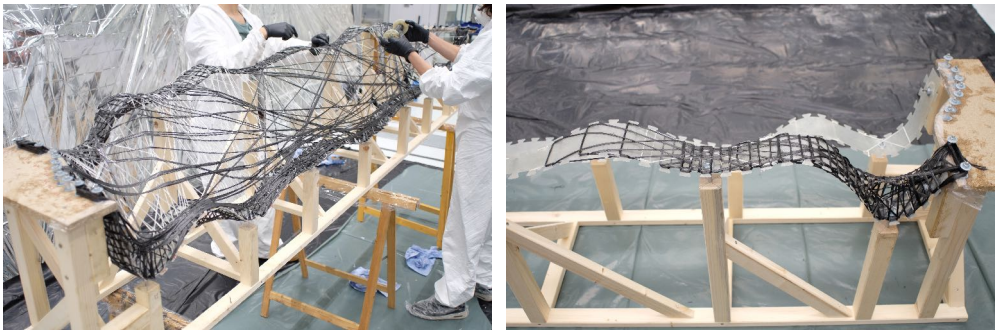

Figure 16: (**a**) Image during the winding of a crease, (**b**) Image of the winding of the infill surface [images by the authors].

4 Results and discussion

The shape optimisation approach developed during this research resulted in a set of hybrid shell designs where three different design-space-to-support scenarios were tested (**fig. 17**). Thanks to the integration of the design constraints during the shape generation, the resulting samples are suitable to be produced with CFW. Furthermore, they comply with the performance criteria established i.e. exhibiting low to near-zero bending and horizontal thrust, having a low height-to-span ratio, and maximizing the use of the shell under tension. Additionally, the wide spectrum of solutions offered by the Pareto front allows for a selection based not only on performance criteria, but also on their architectural impact.

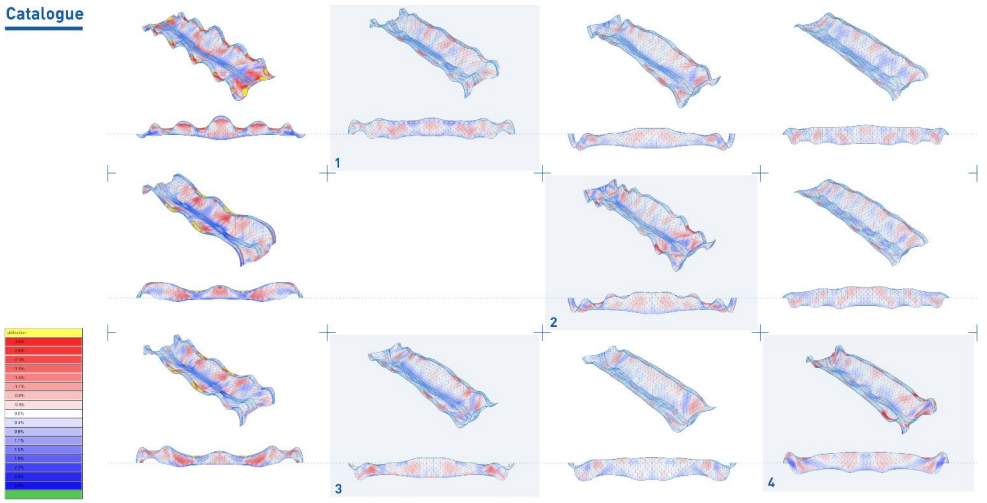

Figure 17: Catalogue of samples from the Pareto front. The ones selected for evaluation are numbered [il. by the authors].

Four shell design samples are selected for evaluation (**fig. 18**). From these candidates, one sample is selected based on a combination of good mechanical performance, simple support condition and spatial quality (determined by the authors

preference). The selected sample is used to generate the filigree model (**fig. 19**) that is later fabricated.

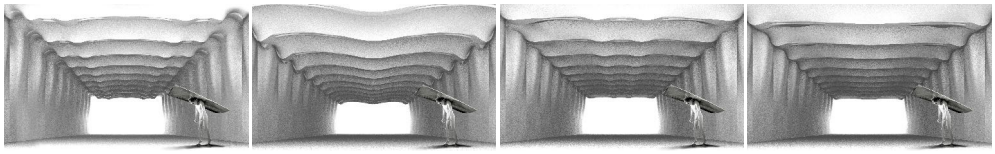

Figure 18: Comparison of the spatial impact of the designs 1 (**a**), 2 (**b**), 3 (**c**) and 4 (**d**) shown in **fig. 17** [il. by the authors].

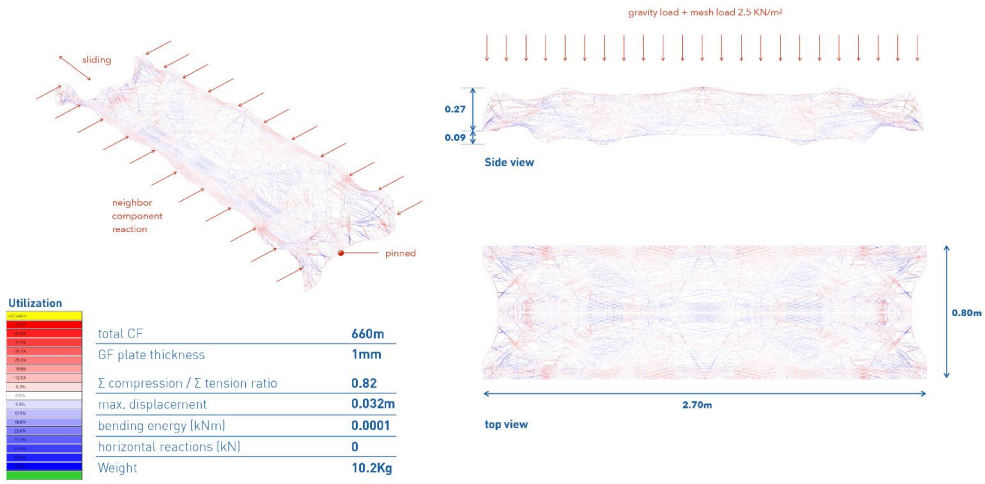

Figure 19: Resulting filigree model [il. by the authors].

A prototype of 2.7 m of span, 80 cm width and 36 cm height is fabricated, weighing 10.2 kg (**fig. 20**). Approximately 660 m of FRP were used in the production of two half-components that are joined mirrored with a stitched connection out of CFRP fibres.

Figure 20: Physical prototype of a Filigree Shell Slab component: (**a**) Top view, (**b**) Side view.

For evaluating the performance of the resulting prototype and compare it with the simulation a non-destructive load test is realized applying up to 559 kg of distributed load. This load is equivalent to 2.54 kN/m^2 i.e. the office load allowance specified previously and no damage was seen to occur at this value (**fig. 21a**). When contrasted with the simulation, the physical prototype exhibits a better performance in terms of vertical displacements and higher self-weight (**tab. 1a**). This is partially attributed to the fact that the GFRP plates and the aluminium sleeves of the supports were not taken into account during the simulation. At the same time, the executed fibre syntax on the creases added a series of members that were also not rendered in the simulation.

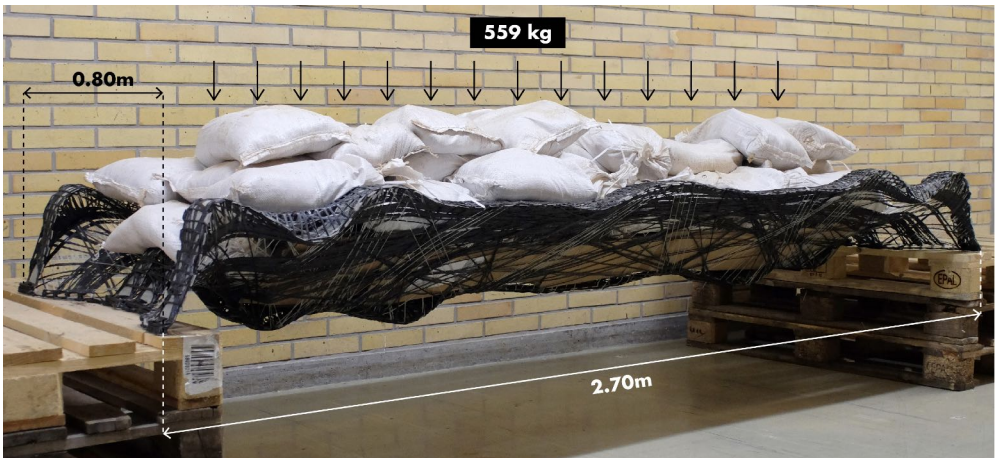

Figure 21: Load testing the prototype.

Item	Simulation	Prototype
Total load (kg)	521,0	559,0
Vertical displacement (mm)	48,1	30,7
Horizontal displacement (mm)	6,2	7,0
Self weight (kg)	4,7	10,2

Table 1: Comparison data obtained from design simulation and physical prototype.

Although the present research focuses on the development of the load-bearing structure of a slab component, a feasible approach for a slab system is illustrated utilizing a lightweight aggregate as a filler to reach the horizontal plane (**fig. 22**). Despite unsolved issues regarding connections and detailing, this approach presents several advantages that are worth noting. The addition of a filler mass provides thermal and acoustic barrier to the filigree load-bearing structure. At the same time, the filler (96.6 percent of the slab volume) can be fully reused once the building ends its service, helping to minimise demolition waste.

With the aim of establishing referential comparisons of such approach, the proposed slab is benchmarked against other prefabricated slab systems (**fig. 23**).

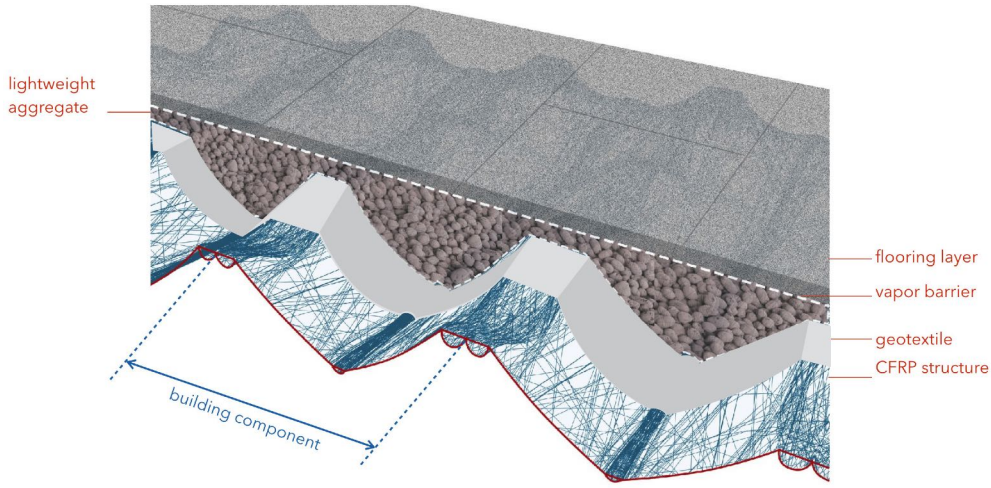

Figure 22: Schematic proposal for a floor slab solution [il. by the authors].

Slab system
benchmarking

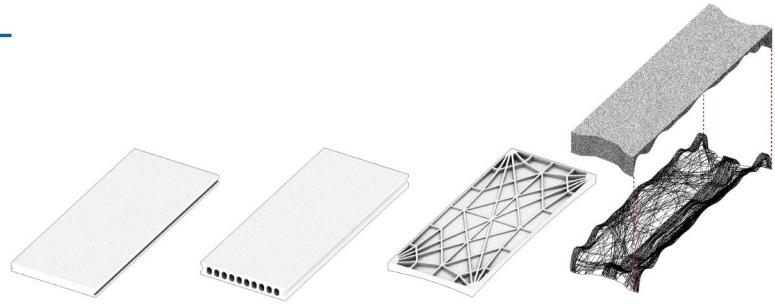

	Solid concrete	Hollow-core	Optimized ribbed vault*	Filigree shell
Size / area	2500x1000x100 / 2.5 m2	2500x1000x150 / 2.5 m2	2500x1000x100 2.5 m2	2700x800x360 / 2.16 m2
Materials	Concrete - steel	Concrete - steel	HPFRC - steel ties	Carbon fiber - expanded clay
Volume	0.25 m³	0.26 m³	0.13 m³	0.014 m3 0.41 m3
Weight	606 Kg	630 Kg	318 Kg	10.2 Kg 131 Kg
Recyclable	- - yes	- - yes	- - yes	- yes
Downcyclable	yes	yes	yes	yes

*Estimations based on López López et al. 2014.

Figure 23: Illustration and table comparing the resulting structure with referential prefabricated slab systems. Solid concrete and Hollow-core are based on standard precast concrete components designed for a similar load and span condition. Optimized ribbed vault based on López López et at. 2014 [il. by the authors].

5 Conclusions

The present research introduced a novel approach to design and manufacturing of coreless filament wound composite structures for slab applications. A multi-stage design process is implemented based on an integrative computational workflow. By thoroughly reviewing the fabrication and slab scenario's constraints, a fabrication-

aware shape optimisation module was implemented and performative shell designs produced. A fibre optimisation module was consequently introduced for generating stress-informed filigree shell models and their associated fabrication data. The above-described method was experimentally evaluated by the realization and testing of a filigree shell slab component, demonstrating the capabilities of this approach for generating performative shell-like designs that can be effectively manufactured with CFW. This experience sets a base for further steps of the implementation of robotically automated production of filigree slab components, where the integration with other building components and the inherent issues of robotic path planning should be addressed. In the same way, this experience expands the lexicon of performative CFW structures towards slab applications and contributes with novel design approach to the research body on fibrous structures carried out by the ICD and ITKE institutes.

Acknowledgements

The project was developed within the ITECH MSc programme at the University of Stuttgart by the first author J.C. under the supervision of the co-authors. Co-authors J.K. and A.M acknowledge the support by the German Research Foundation under Germany's Excellence Strategy – EXC 2120/1 – 390831618.

References

Adriaenssens, S., P. Block, D. Veenendaal, and C. Williams (Eds.) (2014). *Shell Structures for Architecture: Form Finding and Optimization*. London, England: Routledge.

Bletzinger, K.-U. and E. Ramm (2014). *Shell Structures for Architecture: Form Finding and Optimization*, Chapter Computational form finding and optimization. London, England: Routledge.

Brandt-Olsen, C. (2015). Harmonic form-finding for the de- sign of curvature-stiffened shells. Master of philosophy, University of Bath.

Dörstelmann, M., S. Parascho, M. Prado, A. Menges, and J. Knippers (2014). Integrative computational design methodologies for modular architectural fibre composite morphologies. In D. Gerber, J. Sanchez, and A. Huang (Eds.), *Proceedings of ACADIA 2014: Design Agency*, Los Angeles, USA, pp. 219–228. ACADIA / Riverside Architectural Press.

Engel, H. (2007). *Structure Systems*. Stuttgart, Germany: Hatje Cantz.

Felbrich, B., N. Frueh, M. Prado, S. Saffarian, J. Solly, L. Vasey, J. Knippers, and A. Menges (2017). Multi-machine fabrication: An integrative design process utilising an autonomous uav and industrial robots for the fabrication of long-span composite structures. In T. Nagakura, S. Tibbits, C. Mueller, and M. Ibañez (Eds.), *ACADIA 2017*, Cambridge, USA, pp. 248–259. MIT Press.

Knippers, J., V. Koslowski, J. Solly, and T. Fildhuth (2016). Modular coreless filament winding for lightweight systems in architecture. In *CICE 2016 8th International Conference on Fibre-Reinforced Polymer (FRP) Composites in Civil Engineering*, Hong Kong, China.

Koslowski, V., J. Solly, and J. Knippers (2017). Experimental investigation of failure modes of lattice grid composites for building structures based on case studies. In *Proceedings of SAMPE Europe Conference 2017*, Stuttgart, Germany, pp. 201/207. SAMPE Europe.

Malek, S. and C. Williams (2017). The Equilibrium of Corrugated Plates and Shells. *Nexus Network Journal 19*(3), 619–627.

Malek, S. R. (2012). *The Effect of Geometry and Topology on the Mechanics of Grid Shells*. Doctor of philosophy, MIT.

McNeel, R. (2018). Rhino 3d.

Piker, D. (2017). Kangaroo.

Prado, M., M. Dörstelmann, T. Schwinn, A. Menges, and J. Knippers (2014). Core-Less Filament Winding: Robotically Fabricated Fiber Composite Building Components. In W. McGee and M. Ponce de León (Eds.), *Robotic Fabrication in Architecture, Art and Design 2014*, pp. 275–289. Springer.

Preisinger, C. (2018). Karamba 3d.

Solly, J., N. Früh, S. Saffarian, and M. Prado (2018). ICD/ITKE Research Pavilion 2016/2017 : Integrative Design of a Composite Lattice Cantilever. *Creativity in Structural Design: Proceedings of the IASS Symposium 2018* (July).

Vierlinger, R. (2015). Octopus.

Waimer, F., R. La Magna, and J. Knippers (2013). Integrative numerical techniques for fibre reinforced polymers - Forming process and analysis of differentiated anisotropy. *Journal of the International Association for Shell and Spatial Structures 54*(178), 301–309.

Williams, C. (2014). *What is a Shell?*, pp. 21–31. Milton: Routledge.